A Time-Domain Harmonic Balance Method for Rotor/Stator Interactions

Frédéric Sicot[1]
Research Engineer
e-mail: frederic.sicot@cerfacs.fr

Guillaume Dufour
Senior Researcher
e-mail: guillaume.dufour@cerfacs.fr

Nicolas Gourdain
Senior Researcher
e-mail: nicolas.gourdain@cerfacs.fr

Computational Fluid Dynamics Team,
Centre Européen de Recherche et Formation
Avancées en Calcul Scientifique,
42 Avenue Coriolis,
31057 Toulouse Cedex, France

In the absence of instabilities, the large deterministic scales of turbomachinery flows resulting from the periodic rotation of blades can be considered periodic in time. Such flows are not simulated with enough efficiency when using classical unsteady techniques as a transient regime must be bypassed. New techniques, dedicated to time-periodic flows and based on Fourier analysis, have been developed recently. Among these, harmonic balance methods cast a time-periodic flow computation in several coupled steady flow computations. A time-domain harmonic balance method is derived and adapted to phase lag periodic conditions to allow the simulation of only one blade passage per row regardless of row blade counts. Sophisticated space and time interpolations are involved and detailed. The test case is a single stage subsonic compressor. A convergence study of the present harmonic balance is performed and compared with a reference well-resolved classical unsteady flow simulation. The results show, on one hand, the good behavior of the harmonic balance and its ability to correctly predict global quantities as well as local flow pattern; on the other hand, the simulation time is drastically reduced.

1 Introduction

Computational fluid dynamics (CFD) has become a very efficient tool to help engineers design new jet engines. Today, turbomachinery design is mostly based on the assumption of steady flows: The mixing plane technique [1] or frozen rotor [2] simulations are standards in the industry. Motivated by environmental concerns, the Advisory Committee for Aeronautics Research in Europe challenged the civil aircraft industry to reduce the carbon dioxide and noise emissions by half and the nitrogen oxides by 80% in 2020 [3]. The aircraft aerodynamics and the engines have a key role to play in achieving these ambitious objectives. CFD will be of great help, but designers can no longer rely only on steady flow simulations. Indeed, to achieve the performance improvements required, turbomachines are now designed in portions of the design space where blade row interactions play a significant role, such that the classical steady mixing plane approach fails to predict the performance characteristics accurately (see Ref. [4], for instance).

Depending on the spatial and time scales to be resolved, numerous nonlinear time-marching methods are available. Direct numerical simulations and even large eddy simulations are still too expensive with respect to the best computing resources available today to satisfy industrial requirements. So far, unsteady Reynolds-averaged Navier–Stokes (U-RANS) techniques have proved to be the most efficient ones to meet industrial needs. Efficiency is not an absolute notion since it results from a tradeoff between the quality of the physics and the time needed to complete the simulation. In external aerodynamics, U-RANS techniques are generally predictive enough and require relatively short simulation time because of short transient regimes. It is not the case for internal flows yet.

To build an efficient method for unsteady flows, it is interesting to take into consideration all the flow characteristics. Turbomachineries induce time-periodic forced motion of the blades. Even though the chaotic nature of turbulence prevents these flows from being strictly periodic, the largest deterministic scales, the ones engineers are interested in, are also periodic. Several dedicated methods have been developed during the past years. They consider flow variables either in the time domain or in the frequency domain. The frequency-domain techniques are extensively reviewed in Refs. [5,6]. Linearized methods [7] form an important group among these methods. A harmonic perturbation is superimposed over a steady flow, and they do not really rely on a time-marching procedure. Consequently, they are inexpensive to compute. However, when the flow presents strong shock discontinuities and/or unsteady nonlinearities, for instance, the linearity assumption is no longer true (see Ref. [8], for instance). Ning and He [9] extended these techniques to take account of the nonlinearities, yielding the nonlinear harmonic method. This one is limited to only one harmonic of the flow and requires a specific treatment for time stepping. Then, Chen et al. [10] extended it to several harmonics, and He et al. [11] extended it to several frequencies not necessarily multiple of each other for multistage turbomachineries.

In the recent years, similar time-domain methods dedicated to time-periodic flows have been developed. Hall et al. introduced a harmonic balance (HB) method [12], applied to blade cascade computations. Then, Gopinath and Jameson [13] presented the time spectral method (TSM) for external aerodynamic applications. Both methods are essentially similar and allow one to capture the fundamental frequency of the flow and a given number of its harmonics. They cast the unsteady governing equations in a set of coupled steady equations corresponding to a uniform sampling of the flow within the time period. These steady equations can then be solved using standard steady RANS methods with convergence acceleration techniques such as local time stepping, multigrid [14], and implicit schemes. The convergence of a steady flow computation is better mastered than the transient needed by an unsteady flow computation to reach the periodic state since iterative convergence is easier to monitor than time accuracy. This method proved to be efficient in periodic problem computations such as vortex shedding [15,16], flutter [17], helicopter rotor flow [18], and turbomachinery applications [5,19]. The harmonic bal-

[1]Present address: ONERA, The French Aerospace Lab, Aeroelasticity and Structural Dynamics Department, 29 Avenue de la Division Leclerc, BP72, 92322 Chatillon Cedex, France.

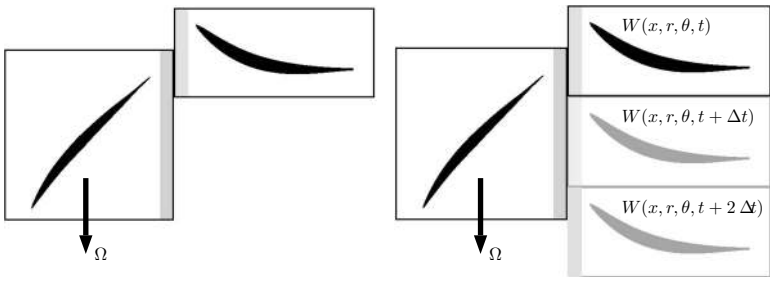

Fig. 1 Blade row interface duplication process (left: relative mesh position; right: duplication with phase lag periodic conditions)

ance approach has also been extended by Ekici and Hall [20,21] to treat several frequencies and has been applied to multiple row configurations, with or without blade vibration

In this paper, a time-domain harmonic balance approach for single stage turbomachines is investigated, where in each blade row, only the frequency (and harmonics) relative to the adjacent blade row is resolved. After presenting the governing equations in Sec. 2, the time-domain harmonic balance formulation is derived (Sec. 3). Then, turbomachinery applications are presented in Sec. 4. The derived HB method is first adapted to the phase lag periodic conditions [22] to allow for the simulation of only one blade passage per row regardless of the blade count of rows. It is then tested on a single stage subsonic compressor (Sec. 5). First, only a radial slice is considered to remove tip leakage flow problems arising in the whole configuration. Then, a procedure to initialize the full 3D computation is given to avoid numerical problems due to the tip leakage flow. Finally, the vortex pattern generated at the tip is analyzed.

2 Governing Equations

The Navier–Stokes equations in Cartesian coordinates are written in semidiscrete form as

$$V\frac{\partial W}{\partial t} + R(W) = 0 \tag{1}$$

W is the vector of conservative variables complemented with an arbitrary number of turbulent variables as within the RANS framework. $R(W)$ is the residual vector resulting from spatial discretization of the convective f_{ci} and viscous f_{vi} fluxes,

$$R(W) = \frac{\partial}{\partial x_i} f_i(W)$$

with $f_i = f_{ci} - f_{vi}$ and

$$f_{ci} = \begin{pmatrix} \rho U_i \\ \rho U_i U_1 + p\delta_{i1} \\ \rho U_i U_2 + p\delta_{i2} \\ \rho U_i U_3 + p\delta_{i3} \\ \rho U_i E + p U_i \end{pmatrix}, \quad f_{vi} = \begin{pmatrix} 0 \\ \tau_{i1} \\ \tau_{i2} \\ \tau_{i3} \\ u \cdot \tau_i - q_i \end{pmatrix}$$

Here, δ denotes the Kronecker symbol. The components of the stress tensor are

$$\tau_{11} = \frac{2}{3}\mu\left(2\frac{\partial U_1}{\partial x_1} - \frac{\partial U_2}{\partial x_2} - \frac{\partial U_3}{\partial x_3}\right), \quad \tau_{12} = \tau_{21} = \mu\left(\frac{\partial U_2}{\partial x_1} + \frac{\partial U_1}{\partial x_2}\right)$$

$$\tau_{22} = \frac{2}{3}\mu\left(-\frac{\partial U_1}{\partial x_1} + 2\frac{\partial U_2}{\partial x_2} - \frac{\partial U_3}{\partial x_3}\right), \quad \tau_{13} = \tau_{31} = \mu\left(\frac{\partial U_3}{\partial x_1} + \frac{\partial U_1}{\partial x_3}\right)$$

$$\tau_{33} = \frac{2}{3}\mu\left(-\frac{\partial U_1}{\partial x_1} - \frac{\partial U_2}{\partial x_2} + 2\frac{\partial U_3}{\partial x_3}\right), \quad \tau_{23} = \tau_{32} = \mu\left(\frac{\partial U_2}{\partial x_3} + \frac{\partial U_3}{\partial x_2}\right)$$

The heat flux vector q components are $q_i = -\kappa \partial T / \partial x_i$, where T is the temperature and

$$\kappa = C_p\left(\frac{\mu_{\text{lam}}}{\text{Pr}_{\text{lam}}} + \frac{\mu_{\text{turb}}}{\text{Pr}_{\text{turb}}}\right)$$

The total viscosity μ is the sum of the laminar μ_{lam} and turbulent μ_{turb} viscosities. Pr_{lam} and Pr_{turb} are the associated Prandtl number. For an ideal gas, the closure is provided by the equation of state,

$$p = (\gamma - 1)\rho\left(E - \frac{U_i U_i}{2}\right)$$

3 Harmonic Balance Method

If the flow variables W are periodic in time with period $T = 2\pi/\omega$, so are the residuals $R(W)$, and the Fourier series of Eq. (1) reads

Table 1 CME2 compressor characteristics

Rotor:stator blade count	30:40
Casing radius	0.275 m
Rotor/stator axial distance	13 mm (hub) 22 mm (casing)
Hub/casing ratio	0.78
Tip gap	0.8% blade span
Rotation speed (nominal point)	6300 rpm (105 Hz)
Mass flow rate (nominal point)	10.5 kg s^{-1}
Pressure ratio (nominal point)	1.14

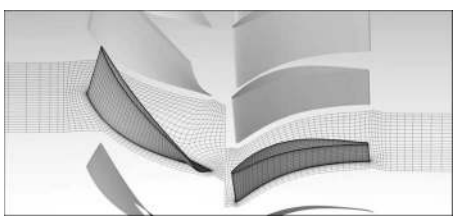

Fig. 2 CME2 Navier–Stokes wall-law mesh (one out of every two points)

(a) first radial plane (b) mid radial plane (c) last radial plane

Fig. 3 Slice mixing plane computation

$$\sum_{k=-\infty}^{\infty} (ik\omega V\hat{W}_k + \hat{R}_k)\exp(ik\omega t) = 0 \tag{2}$$

where $\hat{W}_k$ and $\hat{R}_k$ are the Fourier coefficients of W and R corresponding to mode k. With the complex exponential family forming an orthogonal basis, the only way for Eq. (2) to be true is that the weight of every mode k is zero. An infinite number of steady equations in the frequency domain are obtained as expressed by

$$ik\omega V\hat{W}_k + \hat{R}_k = 0, \quad \forall\, k \in \mathbb{Z} \tag{3}$$

McMullen et al. [23] solved a subset of these equations up to mode N, $-N \le k \le N$, yielding the nonlinear frequency-domain method. As the present HB method has to be implemented in the ELSA solver [24], which is a time-domain solver, Eq. (3) cannot easily be solved.

The HB technique [12] and the TSM [13] use a discrete inverse Fourier transform (DIFT) to cast back in the time domain this subset of $2N+1$ equations from Eq. (3). The DIFT induces linear relations between Fourier coefficients $\hat{W}_k$ and a uniform sampling of W within the period

$$W^* = \mathcal{E}^{-1}\hat{W}^* \Leftrightarrow W_n = \sum_{k=-N}^{N} \hat{W}_k \exp(ik\omega t_n), \quad 0 \le n < 2N+1$$

This leads to a time discretization with a new time operator D_t as follows:

$$R(W_n) + VD_t(W_n) = 0, \quad 0 \le n < 2N+1 \tag{4}$$

These steady equations correspond to $2N+1$ instants equally spaced within the period. The new time operator connects all the time levels and can be expressed analytically by

$$D_t(W^*) = i\mathcal{E}^{-1}\mathcal{D}\mathcal{E}W^* \Leftrightarrow D_t(W_n) = \sum_{m=-N}^{N} d_m W_{n+m} \tag{5}$$

where $\mathcal{D}$ is a diagonal matrix equal to the corresponding wavenumber $\mathcal{D}_{k,k}=k\omega$ and with

$$d_m = \begin{cases} \dfrac{\pi}{T}(-1)^{m+1}\csc\left(\dfrac{\pi m}{2N+1}\right), & m \neq 0 \\ 0, & m = 0 \end{cases}$$

A similar derivation can be made for an even number of instants, but van der Weide et al. [19] proved that it leads to an odd-even decoupling, and as a consequence, the method can become unstable.

A pseudo-time derivative $V\partial W_n/\partial t_n^*$ is added to Eq. (4) in order to time march the equations to the steady-state solutions of all instants. The term $VD_t(W_n)$ appears as a source term that represents a high-order formulation of the initial time derivative in Eq. (1). The pseudo-time marching takes advantage of accelerating methods such as a multigrid technique [14], local time stepping,

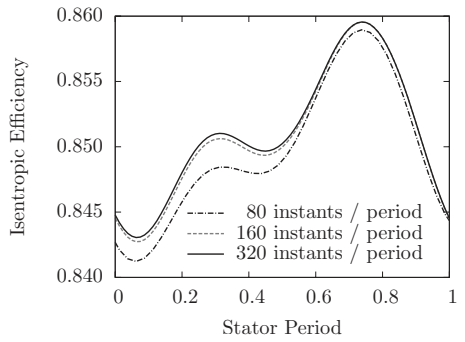

Fig. 4 U-RANS time sampling convergence (isentropic efficiency)

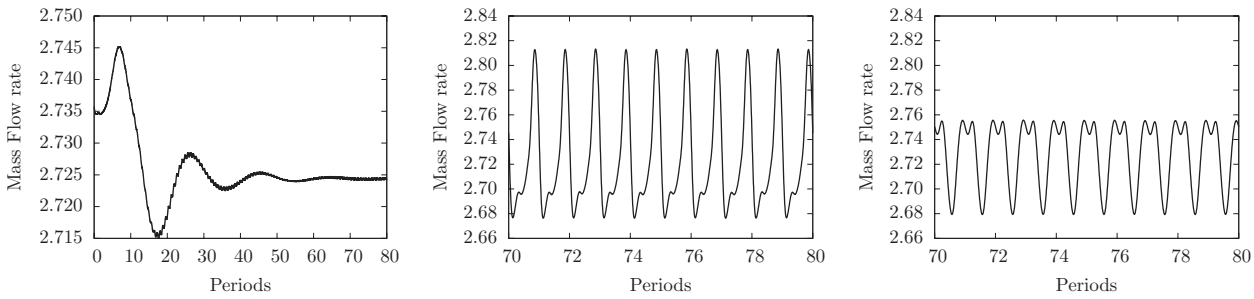

(a) Inlet (b) Blade row interface (c) Outlet

Fig. 5 U-RANS mass flow rate convergence

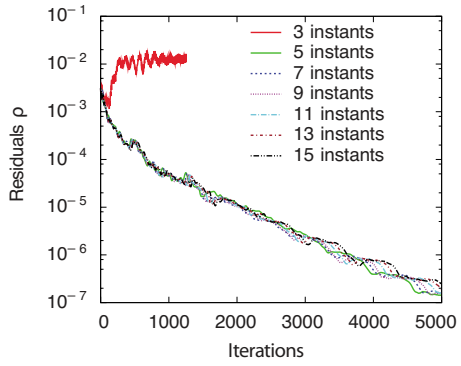

Fig. 6 HB computation residual convergence

and implicit schemes. The latter is carried out by the Block-Jacobi symmetric over-relaxation (BJ-SOR) implicit algorithm developed by Sicot et al. [25].

4 Turbomachinery Boundary Conditions

Turbomachinery simulations are seldom carried out on the whole circumference of the annulus due to the high computational cost. At a stable operating point, the flow shows a spatial periodicity in the azimuthal direction, and thus only a sector of the annulus can be considered in order to reduce the computational domain. Unfortunately, the spatial periodicity of real turbomachineries is often a large fraction of the annulus and sometimes the whole annulus. Using the phase lag periodic conditions (Erdos

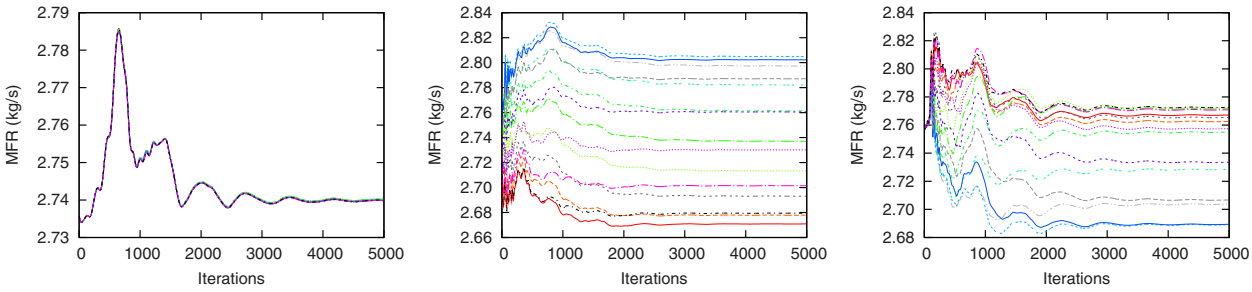

(a) Inlet (b) Blade row interface (c) Outlet

Fig. 7 HB computation MFR convergence (15 instants)

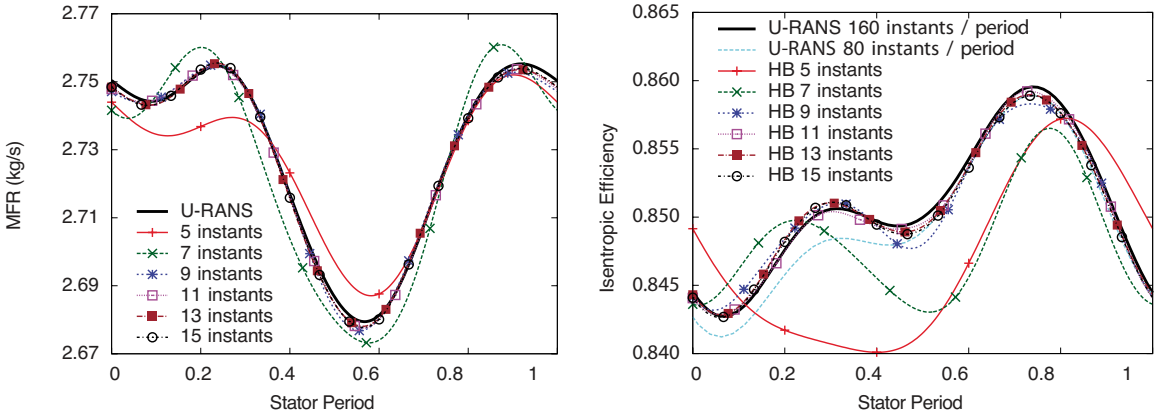

(a) Outlet mass flow rate (b) Isentropic efficiency

Fig. 8 U-RANS and HB comparison: unsteady MFR and efficiency

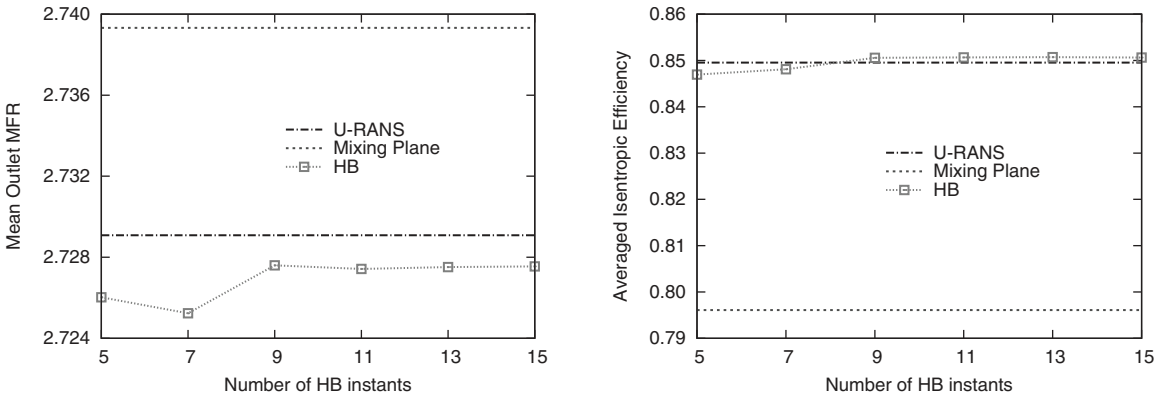

(a) Outlet mass flow rate (b) Isentropic efficiency

Fig. 9 Mixing plane, U-RANS, and HB comparison: time-averaged MFR and efficiency

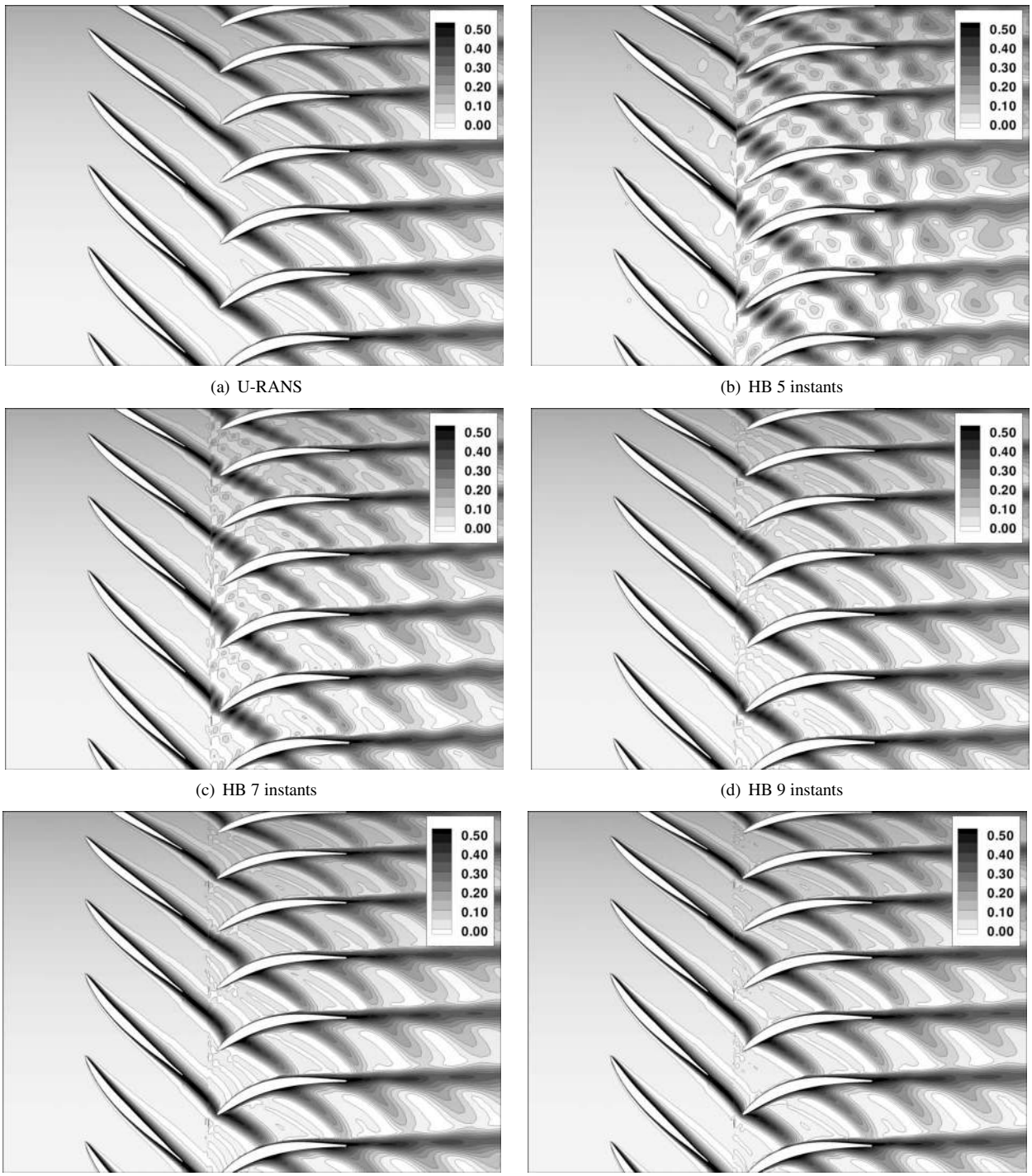

(a) U-RANS

(b) HB 5 instants

(c) HB 7 instants

(d) HB 9 instants

(e) HB 11 instants

(f) HB 13 instants

Fig. 10 Entropy at midspan

et al. [22]), the computational domain can be reduced to a single passage for each row, regardless of the actual blade count.

As a HB simulation ensures the coupling of steady flow computations corresponding to a uniform sampling of the period, a turbomachinery HB simulation is equivalent to coupling frozen rotor computations at different relative positions between the blade rows, sampling a blade passage. It is therefore relevant to initialize a HB simulation with a mixing plane computation so that the wakes propagate into the downstream row at the different HB instants' relative position.

4.1 Phase Lag Periodic Conditions. When solving for only one blade passage of the true geometry, the flow is time-lagged from one blade passage to another. The phase lag periodic condition is used on the azimuthal boundaries of a single blade passage. It states that the flow in a blade passage at time t is the flow at the next passage, but at another time $t+\Delta t$,

$$W(x,r,\theta+\theta_G,t) = W(x,r,\theta,t+\Delta t) \tag{6}$$

This time lag can be expressed as the phase of a rotating wave traveling at the same speed as the relative rotation speed of the

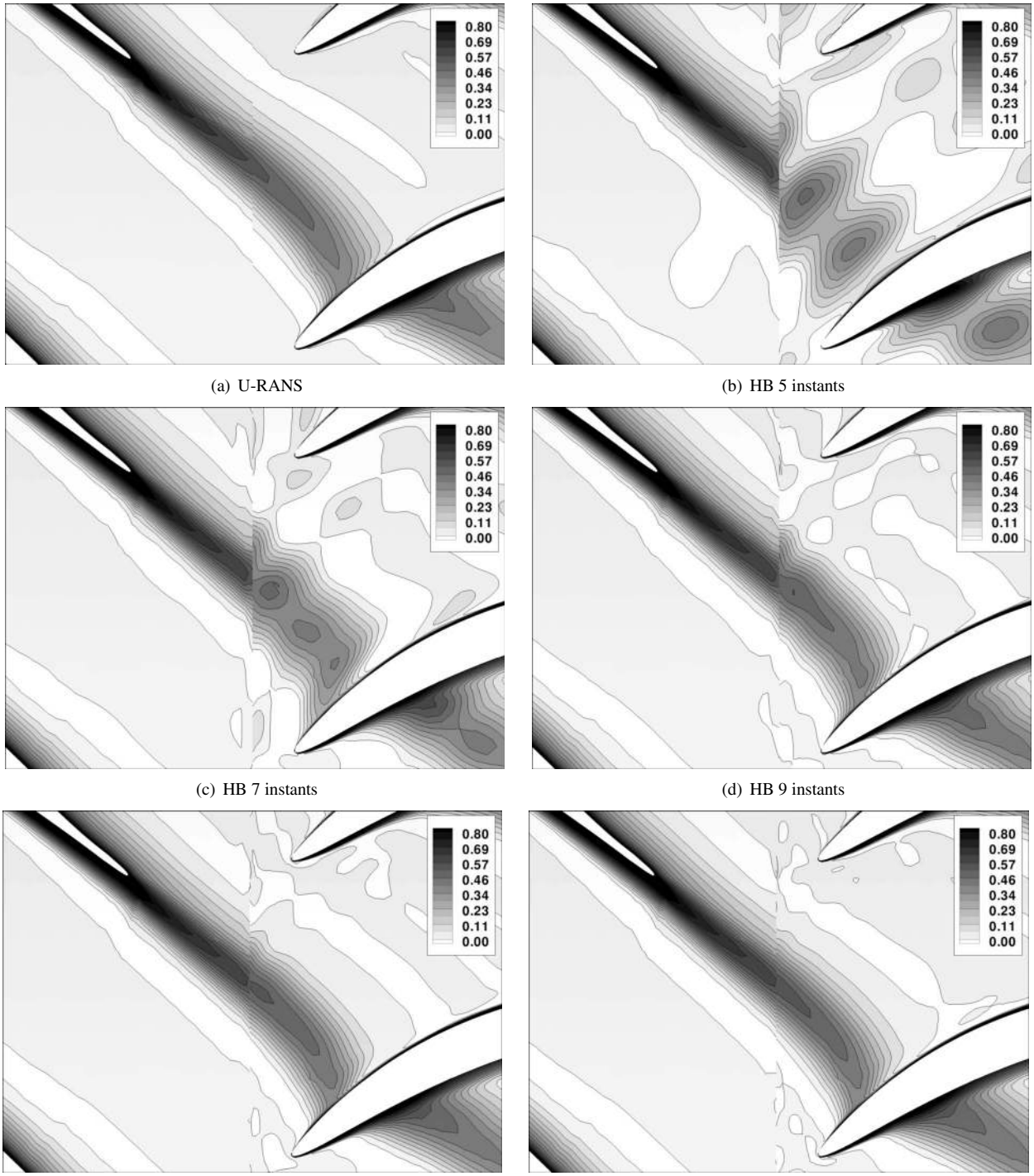

(a) U-RANS (b) HB 5 instants

(c) HB 7 instants (d) HB 9 instants

(e) HB 11 instants (f) HB 13 instants

Fig. 11 Close-up of entropy at midspan at the row interface

opposite row: $\Delta t = \beta / \omega_\beta$. The interblade phase angle (IBPA) depends on each row blade count and relative rotation velocity and is given by Gerolymos et al. [26],

$$\beta = -2\pi \, \mathrm{sgn}(\Omega - \bar{\Omega}) \left(1 - \frac{\bar{B}}{B} \right)$$

The Fourier series of Eq. (6) reads

$$\sum_{k=-\infty}^{\infty} \hat{W}_k(x,r,\theta+\theta_G) e^{ik\omega_\beta t} = \sum_{k=-\infty}^{\infty} \hat{W}_k(x,r,\theta) e^{ik\omega_\beta \Delta t} e^{ik\omega_\beta t}$$

The spectrum of the flow is then equal to the spectrum of the neighbor blade passage modulated by a complex exponential depending on the IBPA,

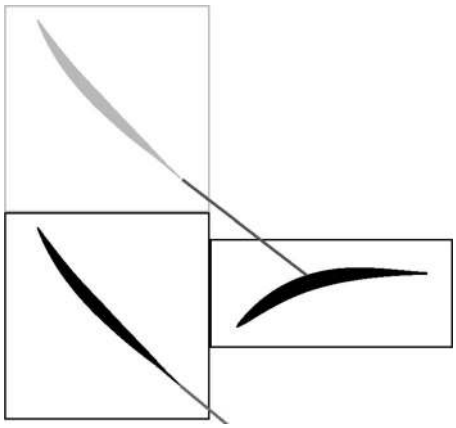

Fig. 12 Downstream row without wake crossing the row interface

$$\hat{W}_k(x,r,\theta+\theta_G)=\hat{W}_k(x,r,\theta)e^{ik\beta}$$

Again, a linear combination of all the time instants can be derived, thanks to spectral interpolation,

$$W^*(\theta+\alpha\theta_G)=\mathcal{E}^{-1}\mathcal{M}\mathcal{E}W^*(\theta)\Leftrightarrow W(x,r,\theta+\alpha\theta_G,t_n)$$
$$=\sum_{m=-N}^{N} b_m W(x,r,\theta,t_{n+m})$$

where $\mathcal{M}$ is a diagonal matrix equal to the IBPA modulation $\mathcal{M}_{k,k}=e^{ik\beta}$ and with

$$b_m=\frac{1}{2N+1}\left(1+2\sum_{k=1}^{N}\cos\left[k\left(2\pi\frac{m}{2N+1}-\alpha\beta\right)\right]\right),\quad \alpha=\pm 1$$

As the HB method solves and stores simultaneously a uniform sampling of the time period, it could be considered similar to Erdos' direct store method. Actually, the method used here is closer to the shape correction developed by He [27], in a sense that the lag is computed, thanks to the Fourier series.

4.2 Row Coupling. Considering only one blade passage per row, the fundamental frequency of a HB computation is the blade passing frequency (BPF) of the opposite blade row $\omega=\bar{B}\Omega$. It means that the time span and thus the time instants solved in each blade row do not match. As a consequence, a time interpolation of the flow in the donor row to the time instants of the receiver row must be performed. A spectral interpolation is achieved in order to preserve the spectrum of the donor row flow,

$$\bar{W}(t)=\mathcal{E}^{-1}\bar{\mathcal{E}}\bar{W}(\bar{t})\Leftrightarrow\bar{W}(t_m)=\frac{1}{2N+1}\sum_{n=0}^{2N}c_{m,n}\bar{W}(\bar{t}_n)\qquad(7)$$

where $\bar{\mathcal{E}}$ considers the opposite row frequencies and time instants $\bar{\mathcal{E}}_{k,n}=(1/(2N+1))\exp(-i\bar{\omega}_k\bar{t}_n)$ and $\mathcal{E}^{-1}$ considers opposite row frequencies to conserve the spectrum but the current row time instant,

$$(\mathcal{E}^{-1})_{m,k}=\exp(i\bar{\omega}_k t_m)=\exp\left(2i\pi\frac{B}{\bar{B}}k\frac{m}{2N+1}\right)$$

The coefficient of Eq. (7) can be derived analytically and read

$$c_{m,n}=1+2\sum_{k=1}^{N}\cos\left[2\pi\frac{k}{2N+1}\left(\frac{B}{\bar{B}}m-n\right)\right]$$

Due to the relative motion between blade rows and the different row pitches, the flow also has to be interpolated in space. This is done, thanks to a totally nonmatching mesh interface [28] performing complex polygon clipping to ensure conservativeness. As shown in Fig. 1, the flow from the stator row has to be duplicated in azimuth in order to provide full information to the rotor row. This duplication has to take the time lag (Eq. (6)) into account.

Finally, to get rid of spurious waves, a filtering is applied in the receiving row, thanks to an oversampling of the donor row. Orszag's criteria [29] state that $3N+1$ instants per time period are sufficient to allow the filtering of aliasing frequencies. For practical reasons, the donor row flow is oversampled at twice the HB computation number of instants, i.e., $4N+2$ instants, satisfying Orszag's criteria, so that the receiver row can keep one out every two samples while filtering. The latter considers the $4N+2$ instants and keeps only the N frequencies of interest,

$$\bar{W}^f=\mathcal{F}^+\mathcal{F}\bar{W}$$

where $\mathcal{F}$ is a rectangular Fourier matrix $(2N+1)\times(4N+2)$ and $\mathcal{F}^+$ is the Moore–Penrose pseudo-inverse of $\mathcal{F}$ ($\mathcal{F}^+\mathcal{F}\neq\mathcal{I}$).

5 Numerical Applications

The present HB method has been implemented in the parallel structured multiblock ELSA solver [24] owned by ONERA, the French Aerospace Lab. The code capability is wide as it can simulate steady and unsteady, internal and external flows, in a relative or fixed motion. It is applied here on the single stage compresseur mono-etage 2 (CME2) subsonic compressor [30], whose characteristics are given in Table 1.

The mesh is shown Fig. 2. The rotor and stator blades are discretized in the streamwise direction by 183 and 171 points, respectively. There are 57 radial planes and 10 in the tip region in the rotor row, leading to a total of 900,000 grid points. No-slip boundary conditions are used in conjunction with wall law. A uniform injection condition is prescribed at the inlet, and a throttle condition with radial equilibrium is used at the outlet.

The second-order scheme with artificial dissipation of Jameson et al. [31] is used for the inviscid terms. The first-order flux splitting of Steger and Warming [32] is also applied on the residual linearization to ensure diagonal dominance of the implicit matrix and thus convergence. A second-order centered scheme is used for the viscous terms. Turbulence is modeled by the transport equation of Spalart and Allmaras [33].

5.1 Radial Slice. A radial slice between 40% and 60% of the blade span is first considered. Five radial planes are retained, comprising 72,000 mesh points. The real geometry is kept so that the blade slice has some twist. This can be clearly seen from the mixing plane computations used to initialize the HB and U-RANS simulations (Fig. 3). At the first radial plane (a), the flow is detached in the stator row, while it is detached in the rotor row at the last radial plane (c). At midspan (b), the flow is correctly attached.

The U-RANS simulation is also carried out on a single blade passage per row using a phase lag periodic assumption and the row interface treatment developed in Ref. [26]. All the computations are resolved with a dual time stepping method [34] with 20 subiterations, and the periodic state is reached within 80 rotor blade passages (more than 2.5 revolutions). A convergence study is performed to get a correct reference. The unsteady isentropic efficiency is plotted (Fig. 4) in the stator time period (linked to the rotor BPF) for different time samplings, namely, 80, 160, and 320 instants per period. The coarsest sampling and the 160-instant sampling provide close results only on the second half of the period. On the first half, the shape is similar but with a gap of about 0.5%. The second sampling is close to the finest sampling of 320 instants per period with an error lower than 0.1% on all the period. Therefore, the U-RANS computation is considered converged with 160 instants per period.

The mass flow rate (MFR) convergence is plotted in Fig. 5. The upstream MFR is the slowest to converge and is thus used to monitor convergence (a). The last ten periods of MFR are then

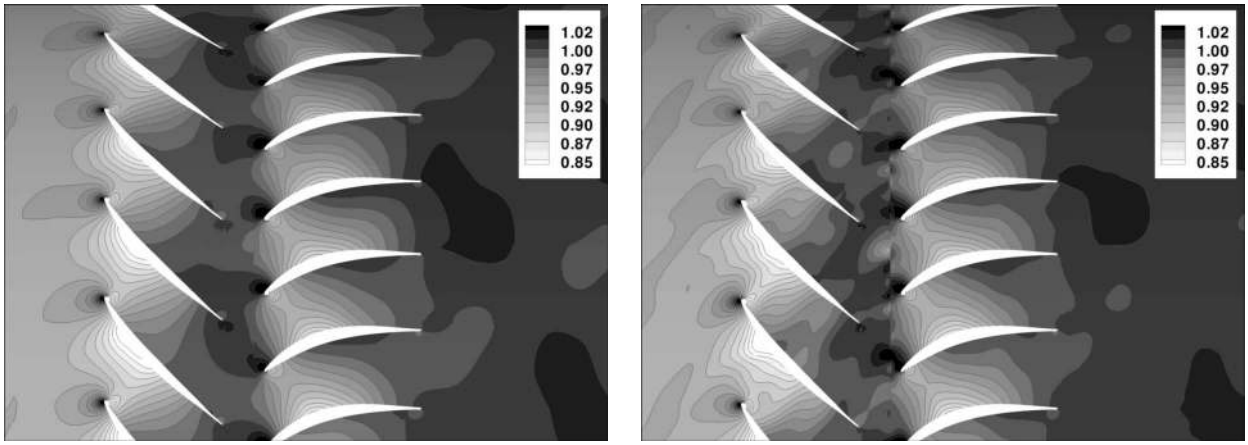

(a) U-RANS (b) HB 5 instants

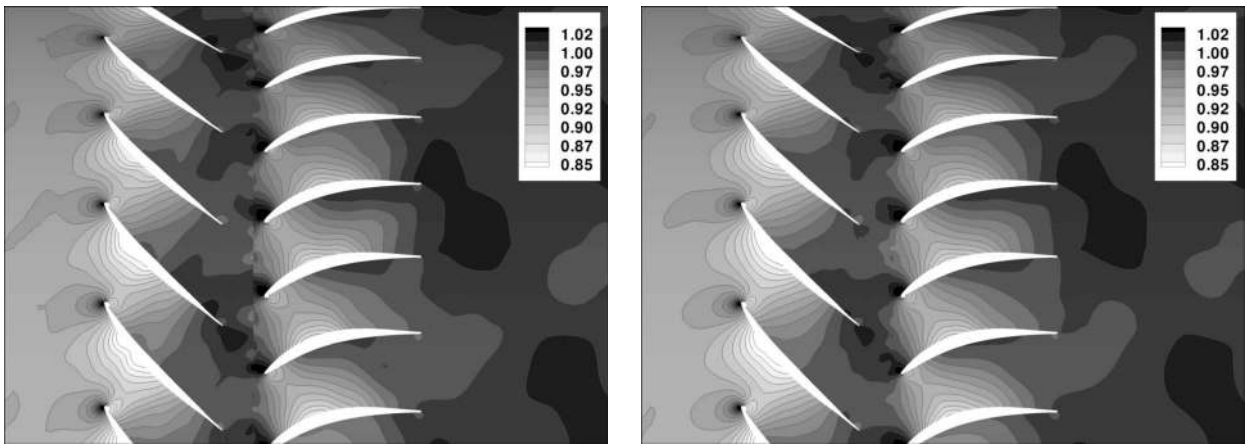

(c) HB 7 instants (d) HB 9 instants

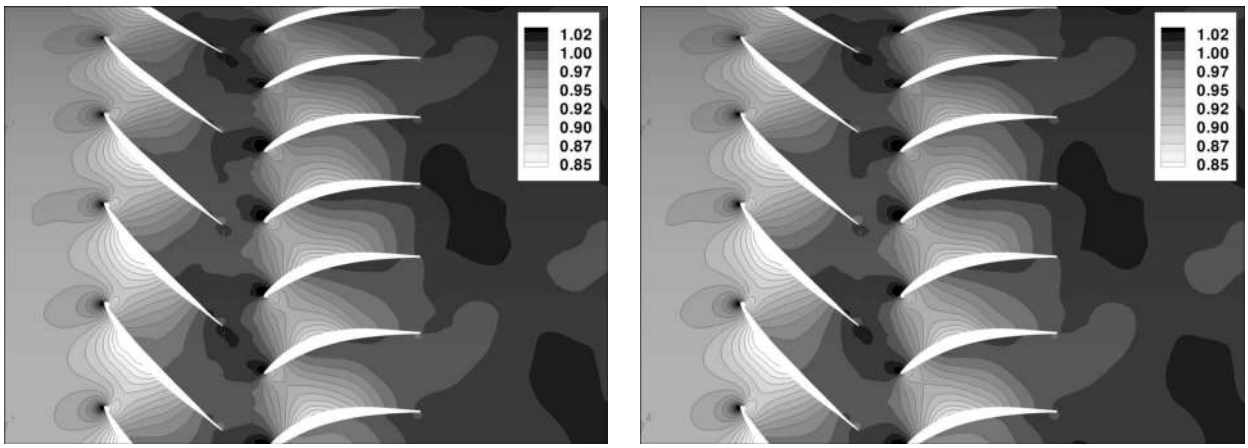

(e) HB 11 instants (f) HB 13 instants

Fig. 13 Pressure at midspan

shown at the mesh row interface (b) and outlet (c).

The residual convergence of the HB simulations is shown in Fig. 6. The three-instant computation fails to converge. The sampling is probably too coarse to provide good space/time interpolations needed by the phase lag periodic conditions and row coupling. For the higher-order computations, the residuals drop about four orders of magnitude in 5000 iterations.

The mass flow rate convergence of the 15-instant HB computation is shown in Fig. 7. As the rotor wakes at the interface have different azimuthal positions for each sample, each solution has a different value of the MFR at the interface (b). This information needs a few hundreds of iterations to reach the inlet and outlet and have these MFRs separate. As in U-RANS, the upstream MFR (a) is the slowest to converge: It does not change any further after 4000 iterations, while the outlet MFR (c) is converged after 3000 iterations.

Figure 8 compares U-RANS and HB unsteady signal of outlet MFR (a) and isentropic efficiency (b). The MFR given by the five-instant HB computation underestimates the amplitude and shows a small lag. Sampling with two more instants slightly overestimates the amplitude, but the trend is closer to the reference U-RANS result. The HB computation with nine instants matches

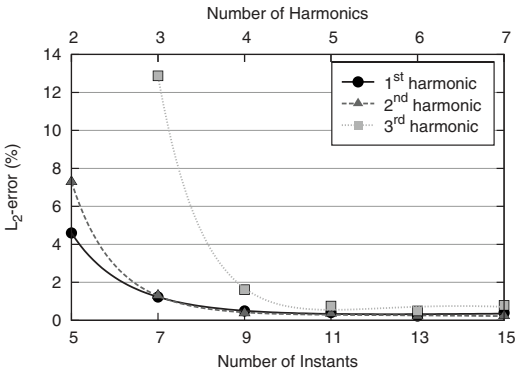

Fig. 14 Wall pressure harmonic convergence

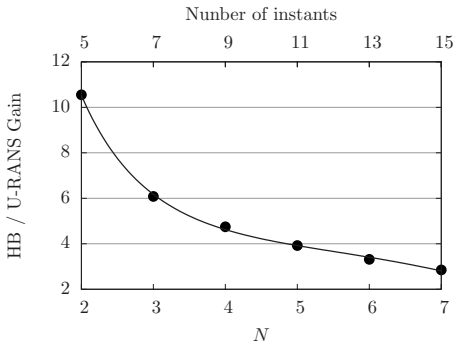

Fig. 15 HB computation CPU time gains

the U-RANS MFR. Beyond 11 instants, all signals are superimposed. The isentropic efficiency curves are more scattered. Five- and seven-instant HB computations give poor results as the aspect is far from the U-RANS prediction. With nine instants, the HB method results are improved and get closer to the U-RANS. The higher-order HB signals are superimposed on the U-RANS with 160 instants per period. The U-RANS made with 80 instants per period (see Fig. 4) is also plotted to show that both methods converge toward the same result and that a HB computation with nine instants already gives a better solution than a poorly resolved U-RANS computation.

The time-averaged MFR and isentropic efficiency are presented (Fig. 9) for the U-RANS and HB computations and compared with the results of the mixing plane computation. The latter overestimates the U-RANS MFR by 0.4%. The five-instant HB computation provides a better estimation with a relative error of 0.1%, which decreases to 0.05% with a sampling of nine instants. The isentropic efficiency predicted by the mixing plane simulation is much lower than the one predicted by the U-RANS. The former underestimates it by 5.5% due to the detached flow at the lowest and highest radii (see Fig. 3). Although the five- and seven-instant HB computations provide poor efficiency (see Fig. 8(b)), their time-averaging give an error lower than 0.2%. With nine instants, the error is decreased by half and does not improve when further increasing the number of instants.

Some instantaneous snapshots of entropy at midspan are shown in Fig. 10. The HB computation with five instants (b) provides a poor pattern of wakes compared with the reference U-RANS simulation (a). Just downstream of the row interface, the wakes are made of sharp and thick bubbles of entropy, which finally dissipate further downstream. This is clearly an effect of the HB method source term (Eq. (5)) together with a coarse time sampling. The nonmatching mesh interface probably adds some numeric noise, as will be shown latter on. Even though the rotor/stator interactions are poorly resolved with five instants, it is noteworthy that the coupling of five steady "frozen rotor" computations can actually capture unsteady flow effects: The wakes are well aligned and at the right position. With seven instants (c), the result is far better. Even if bubbles can still be observed, they are better merged and thinner, and the wake scheme is correct as far as the outlet. The rotor/stator interactions are then well captured.

Figure 11 presents a close-up of the previous entropy snapshots around the blade row interface. The HB computations ((b)–(f)) are based on a totally nonmatching mesh technique (see Sec. 4.2), while the U-RANS (a) transfers Fourier coefficients in both time and azimuthal directions to allow the reconstruction of the field in the opposite row. The five-instant HB computation (b) shows strong discontinuities at the blade row interface. The wake is well formed upstream and then suddenly changes into these sharp bubbles. With seven instants, the contour lines are better aligned with the upstream wakes but still present some bubbles. The wakes are also thicker. With 13 instants, the downstream wake is well formed, but the contour lines are still not perfectly matching. This is a typical behavior of the nonmatching mesh interface implementation used in the present study.

In the present test case, the stator row pitch being lower than the rotor row pitch, it can happen that an instant solved in the stator row is right in the middle of a rotor blade passage; i.e., it does not receive a wake from its interface but rather from its azimuthal boundaries, as sketched in Fig. 12. This can only be recreated by means of the HB time operator and phase lag periodic condition, which need to have enough information from the other instants. So, as the difference of each row pitch increases, the time sampling needs to be finer to compensate for.

The pressure at midspan is presented in Fig. 13. The five-instant HB computation (b) shows a bad pattern especially upstream of the rotor row and at the interface. With seven instants (c), the results are improved upstream of the rotor but remain poor at the interface. Eleven instants (e) are needed to perfectly match the U-RANS reference (a).

The harmonic analysis of the wall pressure on the stator blade is performed, and the $\mathcal{L}_2$-norm of the difference with the U-RANS computation is shown in Fig. 14. The five-instant HB computation captures the first harmonic with a difference of 4.5% with the U-RANS and the second harmonic, the highest mode allowed by such a sampling, with a difference close to 8%. The seven-instant HB computation captures the third harmonic with a difference of 13%. For all harmonics, the trend consists in a rapid decrease in the difference as the sampling gets finer, and it quickly reduces under 1%. Two more comprehensive studies of harmonic behavior of the HB method can be found in Refs. [35,36].

Finally, a HB computation with nine instants gives a good estimate of unsteady general quantities such as mass flow rate and isentropic efficiency. Figure 15 shows the CPU time gains of the HB computations compared with the reference U-RANS computation. A nine-instant HB computation is five times faster. The 11-instant computation perfectly matches U-RANS results and is almost four times faster. Regarding the memory requirement of the method, the gain in computational speed is obtained at the price of an increased storage of data: Since all the instants are solved simultaneously, they are all stored in memory. For the nine-instant case, the memory needed is about nine times that of the classical U-RANS computation, and it scales linearly with the number of instants.

5.2 Full 3D Configuration. Now, the HB method is applied on the full 3D CME2 configuration. Some problems arise from the tip leakage flow, which corrupts all the domain, and the computations fail to converge. It appears to be a transitory problem and can be solved with an appropriate initialization procedure. For instance, Vilmin et al. [37] first computed a solution on a coarse grid with a small number of harmonics. The result is then interpolated to be used as an initial condition to a higher-order computation on the fine grid. This grid/harmonic sequencing strategy allows us to filter errors that appear as high frequencies on the

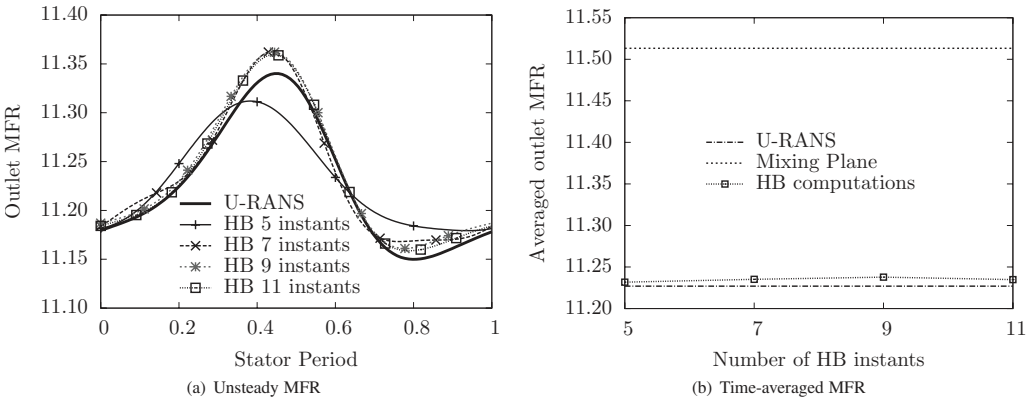

(a) Unsteady MFR (b) Time-averaged MFR

Fig. 16 CME2 mass flow rate

coarse grid and ease convergence on the fine grid. In our case, the mesh is not multigrid compliant. A second initialization procedure is therefore developed: The turbulence is frozen over the mean flow (the HB operator Eq. (5) is no longer applied on the turbulent equations), and the Courant-Friedrich-Levy (CFL) number was drastically lowered by two orders of magnitude. Once the computations pass this transient, the parameters are set back to regular values and the computations converge. It is possible that this problem arises due to some nonsynchronous activity in the tip-gap shear layer, which clearly cannot be accounted for by the present HB method (see Ref. [15] for an example of the need for a well-defined prescribed frequency). Although this is a limitation of the method, the same holds for the classical U-RANS method since the phase lag boundary conditions on the azimuthal frontiers and stage interface filter nonsynchronous unsteadiness as well.

The unsteady MFR is provided Fig. 16(*a*). The HB computations converge faster than those in the slice case since the unsteady MFR signal does not evolve beyond seven instants. The maximum MFR is slightly overestimated compared with the U-RANS. While the five-instant HB computation gives a poor unsteady MFR, it provides the best estimate of time-averaged MFR, as shown Fig. 16(*b*) with a relative error of 0.04% com-

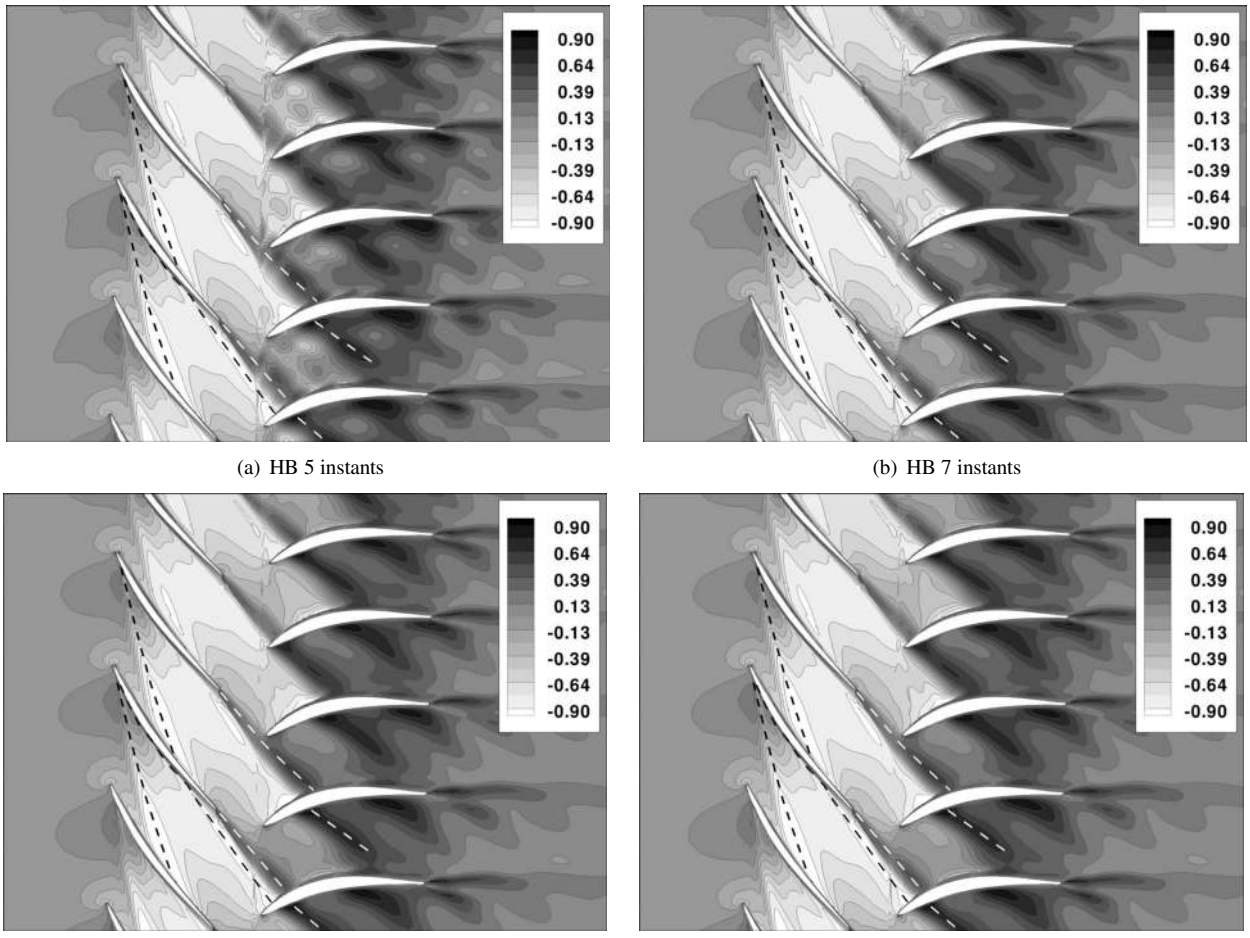

(a) HB 5 instants (b) HB 7 instants

(c) HB 9 instants (d) HB 11 instants

Fig. 17 Instantaneous helicity at constant radius (98% blade span)

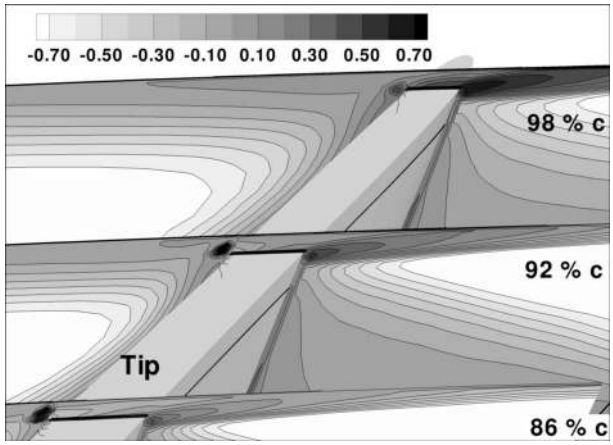

(a) U-RANS

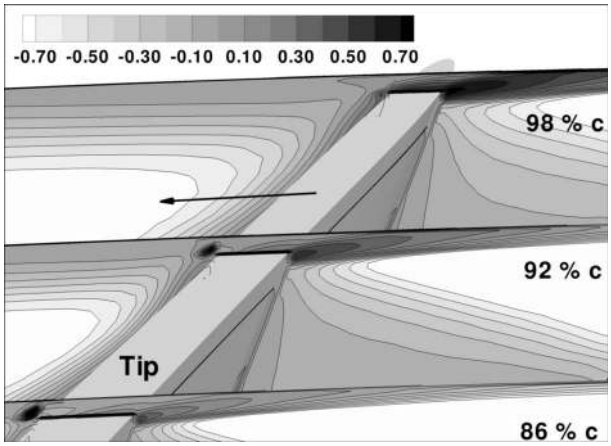

(b) HB 5 instants

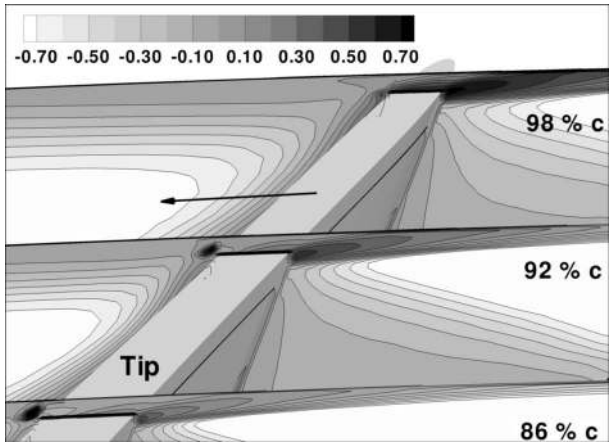

(c) HB 7 instants

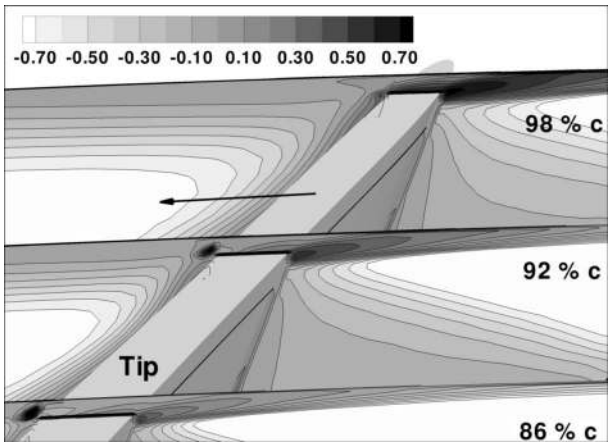

(d) HB 9 instants

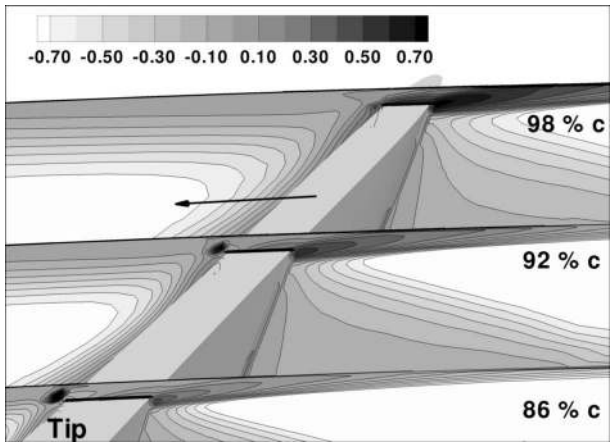

(e) HB 11 instants

Fig. 18 Instantaneous helicity at axial sections

pared with U-RANS. All the other HB computations overestimate the MFR but are nonetheless under 0.1% of error, while the mixing plane simulation overestimates the averaged MFR by 2.55%.

The vortex pattern generated by the tip leakage flow is now investigated. Figure 17 presents instantaneous snapshots of helicity, defined as U rot U, plotted on a blade to blade cut at 98% of the blade span. The helicity is normalized between -1 and 1. These two bounds represent counter-rotating vortices, while zero means no rotation. One can observe a vortex generated at the rotor leading edge impacting the next blade pressure side. Another vortex is present all along the rotor blade suction side and separates at about 80% of the chord. The rotor wakes are made of vortices rotating in the opposite way. Despite the not-so-well-resolved wake pattern of low-order HB computation (which was already observed in Fig. 10), the vortex pattern is well captured for any number of instants. This is probably due to a rather weak unsteadiness.

This is confirmed by Fig. 18, showing some axial cuts at 86%, 92%, and 98% of the rotor blade chord. The black line on the rotor indicates 98% of the blade span, used for the radial cuts of Fig.

17. Another vortex is located close to the casing at the suction side and rotates the opposite way of the ones previously observed. It gets larger as the axial distance grows. Again, all the HB computations ((b)–(e)) provide similar results to the U-RANS computation (a).

6 Conclusions and Prospects

A time-domain harmonic balance method has been derived and adapted to phase lag periodic conditions to reduce the computational domain. A row coupling strategy has been set up, involving time and space interpolations complemented by a filter to remove spurious waves. The derived HB method was first tested on a radial slice of the CME2 single stage compressor. It shows that the HB method is capable of capturing rotor/stator interactions and returns results that are quantitatively similar to a well-converged U-RANS reference computation. However, the convergence depends of the quantities monitored. For instance, the unsteady mass flow rate is well predicted with a number of instants lower than needed for the isentropic efficiency. In the end, the HB method is four to five times faster than the U-RANS for similar accuracy.

The whole 3D configuration shows problems arising with the tip leakage flow. Two initial strategies have been reviewed, and one is tested. The results show that the vortex patterns are well captured.

The HB method is currently being extended to capture several frequencies not necessarily multiple of each other, which is needed for multistage applications where a row is sensitive to different adjacent row blade-passing frequencies. This extension is performed following the work of Gopinath and Ekici but is done purely in the time domain. Since multiple frequency phase lag boundary conditions [38] are not widespread yet in the industry, the multistage HB approach stands as an interesting alternative to full 360 deg computations for multistage turbomachines.

Acknowledgment

This work has benefited from the generous support of the Direction des Programmes Aéronautiques Civils (French civil aviation agency) as part of the Analyze Instationnaire des Turbomachines en aÉrodynamique et aCoustique (AITEC) program. The authors would also like to thank Snecma for its active sponsoring. Finally, Onera, the French aerospace laboratory and owner of the ELSA solver, is greatly acknowledged for its scientific support.

Nomenclature

B = number of blades in a row
E = energy
$\mathcal{E}$ = discrete Fourier transform matrix: $\mathcal{E}_{k,n}=\exp(-i\omega_k t_n)$
k = mode number:$-N\leq k\leq N$
N = number of harmonics
p = pressure
r = radius
$R(W)$ = residuals resulting from space discretization
t, t^*, T = time, pseudo-time, time period
U = flow speed
V = cell volume
W = conservative flow variables: $(\rho,\rho U,\rho E)^\mathsf{T}$
β = interblade phase angle (IBPA)
ρ = fluid density
ω, Ω = angular frequency, rotation speed
θ, θ_G = azimuth, row pitch
a_n = nth instant of the period: $a_n\equiv a(t_n)=a((n/(2N+1))T)$, $0\leq n<2N+1$
$\hat{a}_k$ = kth Fourier coefficient of a: $\hat{a}_k=(1/(2N+1))\Sigma_{n=0}^{2N}a_n\exp(-ik\omega t_n)$, $-N\leq k\leq N$
$\bar{a}$ = property of the opposite row
$a^*(\hat{a}^*)$ = concatenation of all instants (modes) of a: $a^*=(a_0,\ldots,a_{2N})^\mathsf{T}$

References

[1] Denton, J. D., and Singh, U. K., 1979, "Time Marching Methods for Turbomachinery Flow Calculation," *Application of Numerical Methods to Flow Calculations in Turbomachines* (VKI Lecture Series), E. Schmidt, ed., von Kármán Institute for Fluid Dynamics, Rhode-St-Genèse, Belgium.
[2] Brost, V., Ruprecht, A., and Maihöfer, M., 2003, "Rotor-Stator Interactions in an Axial Turbine: A Comparison of Transient and Steady State Frozen Rotor Simulations," Conference on Case Studies in Hydraulic Systems, CSHS03.
[3] Argüelles, P., Lumsden, J., Bischoff, M., Ranque, D., Busquin, P., Rasmussen, S., Droste, B. A. C., Reutlinger, P., Evans, R., Robins, R., Kröll, W., Terho, H., Lagardère, J.-L., Wittlöv, A., and Lina, A., 2001, "European Aeronautics: A Vision for 2020," Advisory Council for Aeronautics Research in Europe, Report.
[4] Trébinjac, I., Kulisa, P., Bulot, N., and Rochuon, N., 2009, "Effect of Unsteadiness on the Performance of a Transonic Centrifugal Compressor Stage," ASME J. Turbomach., **131**(4), p. 041011.
[5] Hall, K. C., Thomas, J. P., Ekici, K., and Voytovich, D. M., 2003, "Frequency Domain Techniques for Complex and Nonlinear Flows in Turbomachinery," 33rd AIAA Fluid Dynamics Conference and Exhibit, AIAA Paper No. 2003-3998.
[6] McMullen, M., and Jameson, A., 2006, "The Computational Efficiency of Non-Linear Frequency Domain Methods," J. Comput. Phys., **212**(2), pp. 637–661.
[7] Verdon, J. M., and Caspar, J. R., 1984, "A Linearized Unsteady Aerodynamic Analysis for Transonic Cascades," J. Fluid Mech., **149**, pp. 403–429.
[8] Dufour, G., Sicot, F., Puigt, G., Liauzun, C., and Dugeai, A., 2010, "Contrasting the Harmonic Balance and Linearized Methods for Oscillating-Flap Simulations," AIAA J., **48**(4), pp. 788–797.
[9] Ning, W., and He, L., 1998, "Computation of Unsteady Flows Around Oscillating Blades Using Linear and Nonlinear Harmonic Euler Methods," ASME J. Turbomach., **120**(3), pp. 508–514.
[10] Chen, T., Vasanthakumar, P., and He, L., 2001, "Analysis of Unsteady Blade Row Interaction Using Nonlinear Harmonic Approach," J. Propul. Power, **17**(3), pp. 651–658.
[11] He, L., Che, T., Wells, R. G., Li, Y. S., and Ning, W., 2002, "Analysis of Rotor-Rotor and Stator-Stator Interferences in Multi-Stage Turbomachineries," ASME J. Turbomach., **124**(4), pp. 564–571.
[12] Hall, K. C., Thomas, J. P., and Clark, W. S., 2002, "Computation of Unsteady Nonlinear Flows in Cascades Using a Harmonic Balance Technique," AIAA J., **40**(5), pp. 879–886.
[13] Gopinath, A., and Jameson, A., 2005, "Time Spectral Method for Periodic Unsteady Computations Over Two- and Three- Dimensional Bodies," 43rd AIAA Aerospace Sciences Meeting and Exhibit, AIAA Paper No. 2005-1220.
[14] Jameson, A., 1983, "Solution of the Euler Equations for Two Dimensional Transonic Flow by a Multigrid Method," Appl. Math. Comput., **13**(3–4), pp. 327–355.
[15] Gopinath, A., and Jameson, A., 2006, "Application of the Time Spectral Method to Periodic Unsteady Vortex Shedding," 44th AIAA Aerospace Sciences Meeting and Exhibit, AIAA Paper No. 2006-0449.
[16] Spiker, M. A., Thomas, J. P., Kielb, R. E., Hall, K. C., and Dowell, E. H., 2006, "Modeling Cylinder Flow Vortex Shedding With Enforced Motion Using a Harmonic Balance Approach," 47th AIAA/ASME/ASCE/AHS/ASC Structures, Structural Dynamics and Materials Conference, AIAA Paper No. 2006-1965.
[17] Thomas, J. P., Dowell, E. H., and Hall, K. C., 2002, "Nonlinear Inviscid Aerodynamic Effects on Transonic Divergence, Flutter, and Limit-Cycle Oscillations," AIAA J., **40**(4), pp. 638–646.
[18] Ekici, K., Hall, K. C., and Dowell, E. H., 2008, "Computationally Fast Harmonic Balance Methods for Unsteady Aerodynamic Predictions of Helicopter Rotors," J. Comput. Phys., **227**(12), pp. 6206–6225.
[19] van der Weide, E., Gopinath, A., and Jameson, A., 2005, "Turbomachinery Applications With the Time Spectral Method," 35th AIAA Fluid Dynamics Conference and Exhibit, AIAA Paper No. 2005-4905.
[20] Ekici, K., and Hall, K. C., 2007, "Nonlinear Analysis of Unsteady Flows in Multistage Turbomachines Using Harmonic Balance," AIAA J., **45**(5), pp. 1047–1057.
[21] Ekici, K., and Hall, K. C., 2008, "Nonlinear Frequency-Domain Analysis of Unsteady Flows in Turbomachinery With Multiple Excitation Frequencies," AIAA J., **46**(8), pp. 1912–1920.
[22] Erdos, J. I., Alznert, E., and McNally, W., 1977, "Numerical Solution of Periodic Transonic Flow Through a Fan Stage," AIAA J., **15**(11), pp. 1559–1568.
[23] McMullen, M., Jameson, A., and Alonso, J., 2001, "Acceleration of Convergence to a Periodic Steady State in Turbomachinery Flows," 39th Aerospace Sciences Meeting and Exhibit, AIAA Paper No. 2001-0152.
[24] Cambier, L., and Veuillot, J., 2008, "Status of the elsA Software for Flow Simulation and Multi-Disciplinary Applications," 46th AIAA Aerospace Sciences Meeting and Exhibit, AIAA Paper No. 2008-0664.
[25] Sicot, F., Puigt, G., and Montagnac, M., 2008, "Block-Jacobi Implicit Algorithms for the Time Spectral Method," AIAA J., **46**(12), pp. 3080–3089.
[26] Gerolymos, G. A., Michon, G. J., and Neubauer, J., 2002, "Analysis and Application of Chorochronic Periodicity in Turbomachinery Rotor/Stator Interac-

tion Computations," J. Propul. Power, **18**(6), pp. 1139–1152.
[27] He, L., 1990, "An Euler Solution for Unsteady Flows Around Oscillating Blades," ASME J. Turbomach., **112**(4), pp. 714–722.
[28] Lerat, A., and Wu, Z. N., 1996, "Stable Conservative Multidomain Treatments for Implicit Euler Solvers," J. Comput. Phys., **123**(1), pp. 45–64.
[29] Orszag, S. A., 1971, "On the Elimination of Aliasing in Finite-Difference Schemes by Filtering High-Wavenumber Components," J. Atmos. Sci., **28**(6), p. 1074.
[30] Michon, G. J., Miton, H., and Ouayahya, N., 2005, "Experimental Study of the Unsteady Flows and Turbulence Structure in an Axial Compressor From Design to Rotating Stall Conditions," Sixth European Turbomachinery Conference.
[31] Jameson, A., Schmidt, W., and Turkel, E., 1981, "Numerical Solutions of the Euler Equations by Finite Volume Methods Using Runge-Kutta Time-Stepping Schemes," AIAA 14th Fluid and Plasma Dynamic Conference, AIAA Paper No. 81-1259.
[32] Steger, J. L., and Warming, R. F., 1981, "Flux Vector Splitting of the Inviscid Gas-Dynamic Equations With Applications to Finite Difference Methods," J. Comput. Phys., **40**(2), pp. 263–293.
[33] Spalart, P. R., and Allmaras, S. R., 1992, "A One-Equation Turbulence Transport Model for Aerodynamic Flows," 30th AIAA Aerospace Sciences Meeting and Exhibit, AIAA Paper No. 92-0439.
[34] Jameson, A., 1991, "Time Dependent Calculations Using Multigrid, With Applications to Unsteady Flows Past Airfoils and Wings," Tenth Computational Fluid Dynamics Conference, AIAA Paper No. 91-1596.
[35] Sicot, F., Dufour, G., and Gourdain, N., 2009, "Discrete-Frequency Noise Prediction Using a Harmonic Balance Method," 19th International Symposium on Air Breathing Engines, ISABE Paper No. 2009-1131.
[36] Posson, H., Sicot, F., Moreau, S., and Gourdain, N., 2010, "Comparison of Analytical and Numerical Predictions of Stator Vane Pressure Distribution Produced by Mean Rotor Wake Impingement," 13th International Symposium on Transport Phenomena and Dynamics of Rotating Machinery.
[37] Vilmin, S., Hirsch, C., Lorrain, E., and Swoboda, M., 2006, "Unsteady Flow Modeling Across the Rotor/Stator Interface Using the Nonlinear Harmonic Method," ASME Turbo Expo, Paper No. GT-2006-90210.
[38] He, L., 1992, "A Method of Simulating Unsteady Turbomachinery Flows With Multiple Perturbations," AIAA J., **30**(11), pp. 2730–2735.